In situ observation of the indentation-induced phase transformation of silicon thin films

Y. B. Gerbig,[1] C. A. Michaels,[2] A. M. Forster,[3] and R. F. Cook[1]
[1]*Ceramics Division, National Institute of Standards and Technology, Gaithersburg, Maryland 20899, USA*
[2]*Surface and Microanalysis Science Division, National Institute of Standards and Technology, Gaithersburg, Maryland 20899, USA*
[3]*Materials and Construction Research Division, National Institute of Standards and Technology, Gaithersburg, Maryland 20899, USA*

(Received 2 December 2011; revised manuscript received 26 January 2012; published 5 March 2012)

Indentation-induced phase transformation processes were studied by *in situ* Raman microspectroscopy of the deformed contact region of silicon on sapphire samples during contact loading and unloading. During loading, the formation of Si-II and another phase, indentified as the bct5 structure, was observed, thus providing experimental evidence for both the existence of the bct5 phase and the possibility of generating this phase under indentation conditions. The pressure dependence of the Raman phonon frequencies for the bct5 modes was determined. During unloading, the transformation of the bct5 phase into the metastable bc8 (Si-III) and r8 (Si-XII) structures was observed. The measurements indicated that bc8 can form simultaneously with the r8 structure in indentation tests rather than subsequently from r8 in a separate process as previously assumed.

DOI: 10.1103/PhysRevB.85.104102 PACS number(s): 64.70.K−, 78.30.Am, 62.20.F−

I. INTRODUCTION

Silicon (Si) in its pristine diamond cubic (dc) phase can be transformed to different crystallographic structures through the application of mechanical stress. As the modification to the crystallographic structure of Si, the basic component of most electronic circuits and microelectromechanical system (MEMS) devices, is often connected to a change in its mechanical,[1] electrical,[2] chemical,[3] or optical properties,[4] the phase transformation of Si has been extensively studied. At hydrostatic pressures of 10–13 GPa, Si undergoes a nonmetallic→metallic transition, as the initial dc structure of Si-I [Fig. 1(a)] transforms to the denser body-centered-tetragonal β-tin structure of the Si-II phase [Fig. 1(b)], with a subsequent increase in Si coordination from fourfold to sixfold.[5] Further compression leads to a sequence of transitions to other metallic phases according to several theoretical studies and quasihydrostatic diamond-anvil cell (DAC) experiments.[6] On release of the hydrostatic pressure, the high-pressure phases do not recover to the dc structure but to other metastable phases in which Si is fourfold coordinated but are denser than the dc phase.[6] Slow decompression from the β-tin phase leads to the rhombohedral r8 (Si-XII) phase [Fig. 1(d)] at about 10 GPa, which subsequently transforms to the body-centered-cubic bc8 (Si-III) phase [Fig. 1(e)] at about 2 GPa.[7,8]

Shear stress has been reported to lower the threshold pressures for phase transformations in Si.[9] Shear is critical in the initiation of phase transformations while hydrostatic pressure plays an important role in the further development of phase changes after initiation.[10] Furthermore, it has been speculated that shear stresses may promote the formation of phases not observable under hydrostatic conditions.[11,12] To investigate the Si phase transformation in the presence of shear stress, many indentation studies employing various auxiliary characterization techniques, such as atomic force microscopy,[13,14] scanning electron microscopy,[1,15,16] transmission electron microscopy,[14,17–20] and Raman microspectroscopy,[14–16,21–23] have been conducted in recent years. It was found that the phase transformation on pressure release is influenced by the unloading rate; at slow rates, a mixture of bc8 and r8 phases was detected, while for fast unloading rates, mostly amorphous silicon (a-Si) was detected in the residual contact impressions.[16,21] The presence and distribution of residual phases in indentations can be linked to the crystallographic anisotropy and inhomogeneity of the stress distribution.[22,24]

In conventional indentation experiments, the structure and phase of the material is probed only after the completion of the indentation test (*ex situ*), which leaves room for speculation on the exact path of transformation for indented Si, as the presence of intermediate phases cannot be directly observed. To date, the only possibilities for *in situ* observations of indentation-induced phase transformation are based on measurements of the electrical resistance of the contact between a probe tip and the indented Si surface by either scanning spreading resistance microscopy[12,25] or by indentation with a conductive tip.[2,26–30] The conductivity of Si phases can range from semiconductor to metal-like,[2,31] and hence variations in the contact resistance can be an indirect indicator for the transformation processes occurring within the contact region. *In situ* electrical measurements have determined that the semiconductorlike dc phase transforms during loading into material of more metallic (conducting) character,[2,26–29] which is believed to be β-tin based on the transformation sequences observed in quasihydrostatic DAC tests.[28,29] Simulations of indentation experiments suggest that the dc crystal lattice of Si transforms into various body-centered-tetragonal (bct) structures with both sixfold (β-tin) and fivefold coordination (bct5) during loading.[25,32–35] Boyer *et al.*[11] postulated that shear strain is essential to the formation of the bct5 phase [Fig. 1(c)], which would explain why this phase has not been observed under pure hydrostatic conditions. As bct5 is, as β-tin, metallic,[36] the reported changes in *in situ* electrical measurements during loading[2,26,27] could be related to the formation of either or both of those phases.

During the unloading segment of *in situ* electrical measurements, a sudden change in the contact resistance indicated further transformations in crystallographic structure, which is assumed to be connected to the formation of an r8-bc8 mixture or a-Si dependent on the direction of change in the resistance.[37] However, as multiple phases (sometimes with similar electrical properties) can coexist in the transformation region

 ©2012 American Physical Society

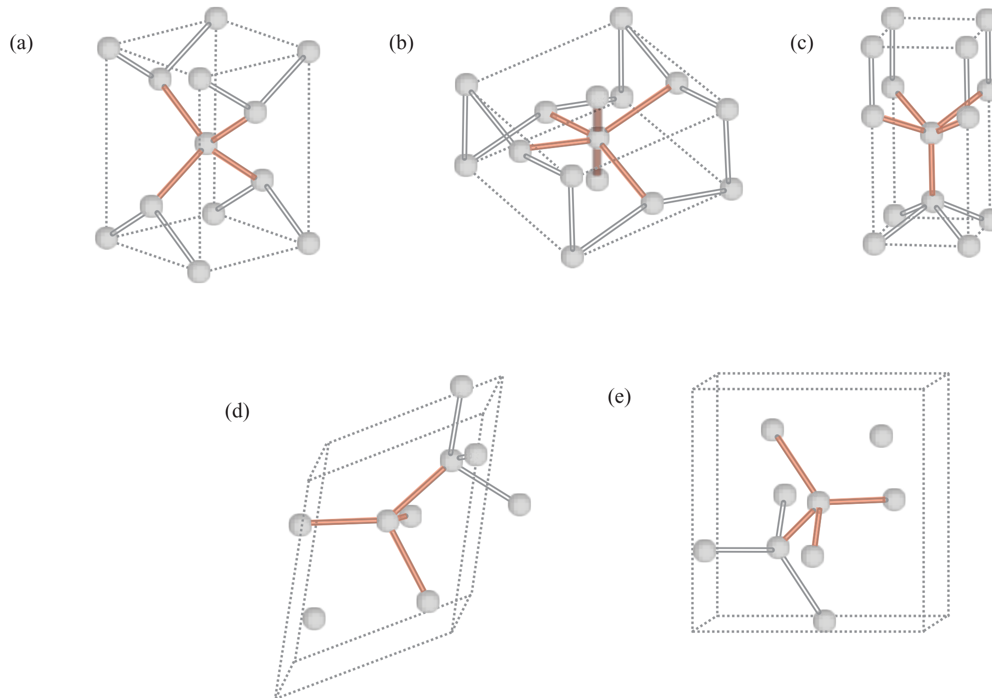

FIG. 1. (Color online) Ball and stick crystallographic structure diagrams of Si phases observed during indentation experiments: (a) dc (Si-I), (b) β-tin (Si-II), (s) Si-bct5, (d) r8 (Si-XII), (e) bc8 (Si-III). For illustration purposes, more atoms are shown than comprised in the actual unit cell for some phases.

depending on the unloading conditions,[16,21] the unambiguous identification of phases is very difficult with *in situ* electrical probing. In order to directly analyze indentation-induced Si phase transformations, a probe technique able to identify the crystallographic structure of various phases, such as Raman spectroscopy, must be employed.

This paper reports direct observation of the phase transformation cycle induced by indentation in Si thin films. The study was conducted on an indentation device specifically designed to couple with a Raman microscope, which enables the *in situ* analysis of strains (and pressures) and phases in the mechanically deformed region under contact loading.

II. EXPERIMENTAL DETAILS

In order to perform an *in situ* Raman analysis of Si phase transformation, a thin Si film was indented while simultaneous collecting Raman measurements.

A. Test specimen

The *in situ* tests were performed on a Si on sapphire (SOS) specimen (manufacturer: Valley Design Corporation, Vera Cruz, CA).[38] The epitaxially grown Si(100) film was 600 nm $\pm$ 60 nm thick and was deposited on a sapphire (r-plane) substrate of thickness of 530 μm $\pm$ 50 μm and polished on both sides. (Uncertainties represent manufacturer specifications.) The surface normal of the sample was misaligned by $5^\circ \pm 1^\circ$ with respect to the $\langle 001 \rangle$ direction of the Si film. The sample (20 mm $\times$ 20 mm) was cut from a SOS wafer. The cut edges of the sample were misaligned by $3.5^\circ \pm 1^\circ$ with respect to the directions $\langle 110 \rangle$ and $\langle 1\bar{1}0 \rangle$ of the film, as shown by electron backscattering diffraction (EBSD) measurements. (Uncertainties represent intrinsic measurement errors and mounting errors.) The substrate normal was designated the Z direction and the Si directions $\langle 110 \rangle$ and $\langle 1\bar{1}0 \rangle$ were designated the X and Y directions, respectively, as employed for the Porto notation[39] used to describe the Raman spectra.

B. Indentation device

The tests were conducted on an indentation device specifically designed to couple to a microscope enabling *in situ* Raman measurements of mechanically deformed regions in materials, as shown in Fig. 2. The indentation device consists of a voice coil linear actuator (VCLA), linear variable differential transformer (LVDT) sensor, and an indenter tip suspended by copper-beryllium orthogonal springs. All of these components are installed in a metal frame which is mounted to the X-Y translation stage of the microscope, along with the specimen holder.

Adjustment screws on the metal frame were used for coarse, manual vertical positioning of the indenter tip. The VCLA was employed for the fine positioning of tip, whereby the orthogonal springs ensured the linearity and repeatability of the movement.[40] The VCLA also generated the force applied to the indenter tip. The open-loop control system, to which the VCLA was connected, enabled a defined adjustment of indentation cycle (loading and unloading rates, maximum force, hold time period). The displacement of the tip was measured with the LVDT sensor.

The raw data collected during the indentation (LVDT voltage, current applied to VCLA) were processed through a data acquisition system and converted to force and displacement

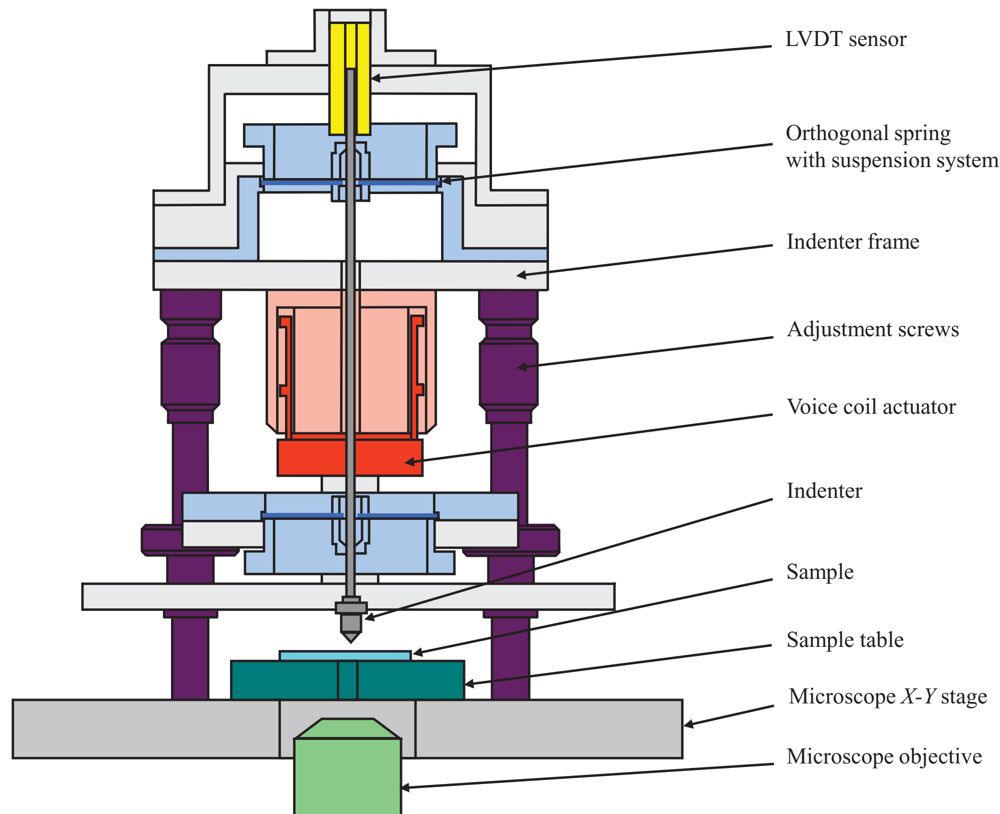

FIG. 2. (Color online) Schematic cross-sectional diagram of the indentation device used in the *in situ* Raman measurements.

values. The conversion algorithms were determined prior to the measurements by calibration of the device with a load cell and micrometer screw.

The specimen holder was attached to the microscope stage with magnets and featured an aperture in the center, which allowed the Raman excitation laser to be focused through the transparent specimen into the sample region in contact with the indenter tip.

C. Raman microscope

The Raman microscope is based on a commercial inverted microscopy platform (Olympus IX-71, Center Valley, PA)[38] with a mirror unit turret containing conventional white light imaging optics and a laser port for entry of the 785-nm wavelength laser excitation beam and collection of the scattered Raman light. The white light imaging capability was critical for colocating the tip, sample, and excitation beam such that the collected Raman spectra were emitted from the sample region in contact with the indenter tip. A 50×, 0.55 numerical aperture (NA) ultralong working distance metallurgical objective was used for both the white light imaging and Raman microscopy. The estimated laser spot size ($\sim$1 μm) was smaller than the radius of curvature of the indenter tip. The estimated depth of field for the collection of Raman photons ($\sim$10 μm) was much greater than the Si layer thickness, as shown in Fig. 3.

A detailed description of the 785-nm light source and Raman spectrometer has been reported previously.[41] Output from the source was fiber coupled to a modified Raman probe head (Kaiser Optical Systems, Ann Arbor, MI)[38] that contained a collimation optic, a polarizer, a narrow bandpass holographic transmission grating, and a spatial filter on the excitation arm. The collimated output of the probe head was steered into the laser port and was reflected from a beamsplitter into the pupil of the objective where it was focused onto the top surface of the Si. The power level at the sample for these measurements was 5 mW. The beamsplitter transmitted a small amount of 785-nm light through to the white light camera allowing for visualization of the focused laser spot, facilitating the process of aligning the beam with the tip.

The scattered Raman light was collected by utilizing the same objective and was reflected from the beamsplitter and directed back into the probe head, where it passed through a holographic notch filter and a long pass filter for Rayleigh rejection, through a polarization analyzer, and was subsequently coupled into a multimode optical fiber for delivery to the aforementioned spectrometer. In all measurements reported here the polarizers for the excitation and detection arms were set parallel, providing $ZYY\bar{Z}$ spectra in Porto notation. The 50-μm core diameter of the fiber served as the confocal aperture. An 805-nm diode laser was coupled into the collection fiber in reverse to allow for visualization of the fiber core image in the microscope focal plane for the purpose of insuring optimal microscope alignment. Raman light scattered at wave numbers below 200 cm^{-1} was not collected as it was blocked by the long pass Rayleigh blocking filter utilized in the microscope.

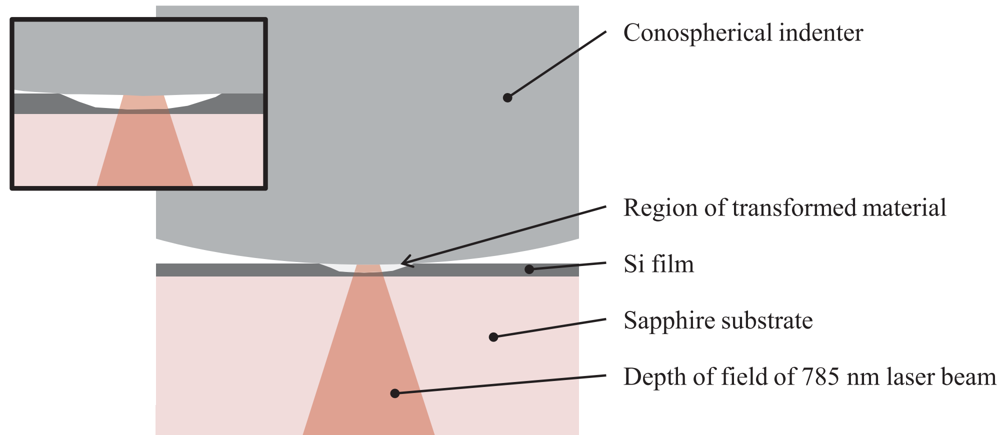

FIG. 3. (Color online) Schematic drawing of the cross section of the deformed contact region to illustrate the relative proportions of deformed region and depth of field of the Raman microscope. The inset shows a closeup of the contact region.

D. Indentation experiments

In order to collect the Raman spectra at defined contact pressures, the *in situ* experiments were conducted as a stepped indentation test; a defined indentation force was applied and held at that value for 3 min to allow acquisition of the Raman spectrum. The indentation force was then changed to the next value. This cycle was repeated throughout the loading and unloading segments of the experiment. The maximum force applied during the indentation experiments was approximately 550 mN. The indenter was a conospherical diamond tip with a tip curvature of 50 μm. In this geometry, the deformed region under the tip was sufficiently large to allow focusing of the incident laser and collection of measurements even at small forces (i.e., during the early stages of the *in situ* indentation test).

Indentation experiments were also conducted under continuous loading and unloading conditions on a commercial nanoindentation device that featured a similar frame stiffness but greater displacement resolution compared to the *in situ* indenter. Discontinuities in the force-displacement curve related to the phase transformation were more pronounced and were identified more easily with the commercial instrument. The same indenter tip as used with the *in situ* indenter was installed on the commercial device. The maximum indentation force was the same as that used in the *in situ* experiments, and the loading and unloading rates were comparable to those used in the *in situ* experiments.

E. Analysis of Raman spectra

The experimental Raman spectra were fit to model functions composed of sums of Voigt line shapes using the supervised nonlinear least-squares peak fitting routine available in the commercial spectral analysis package GRAMS.[38]

The fitting procedure was complicated by the fact that the 378 cm^{-1} peak associated with the sapphire substrate was located in the same frequency range as Raman modes linked to the high-pressure Si phases. However, it has been shown that the position of the 378 cm^{-1} peak exhibits a pressure dependency similar to the 418 cm^{-1} peak of sapphire.[41–43] As the position of latter peak does not shift during the indentation cycle (see Fig. 5 later), the position of the 378 cm^{-1} peak was also assumed to be constant. Hence, the frequencies of these peaks were fixed at 378 and 418 cm^{-1}, respectively, when fitting the Raman spectra to determine the positions of Si peaks.

F. Determination of the contact pressure, peak indentation strain, and unloading strain rate

The mean contact pressure $p_{\rm i}$ at the spherical indenter-flat sample interface was calculated for a specific indentation force using the equation $p_{\rm i} = F_{\rm i}/(\pi a_{\rm c,i}^2)$, where $a_{\rm c,i}$ is the radius of the circle of contact at the force $F_{\rm i}$. The radius of the circle of contact was determined at a specific indentation force following the approaches employed by Weppelman *et al.*[44] (loading segment) and Field *et al.*[45] (unloading segment) of the indentation.

The characteristic indentation strain is $\varepsilon_{\rm I} = 0.2(h_c/a_c)$, where $h_{\rm c}$ is the indentation contact depth and a_c is the contact radius.[46] The peak indentation strain is the strain value when the peak (maximum) indentation force is applied to the sample. For a spherical indentation, $(h_{\rm c}/a_c) \approx (a_c/R)$, where R is the indenter radius. For the conditions used in this paper on Si, $a_c \approx 4.5$ μm and $R \approx 50$ μm to give $\varepsilon_{\rm I} \approx 0.018$ at maximum indentation force. The unloading strain rate was $\dot{\varepsilon}_I < 10^{-3}$ s^{-1}.

III. RESULTS

Figure 4 shows a typical force-displacement curve recorded by the commercial indentation device on the SOS sample. The circled data points indicate the indentation forces at which Raman spectra were collected during the *in situ* experiment. Due to significant less noise in the displacement channel of the commercial indentation device, the displacement data required for calculating contact pressures (see Sec. II) were determined from the indentation curve obtained with this device. Figure 5 summarizes the Raman spectra collected in the contact region during indenting the SOS sample as function of the contact pressure. The spectrum of the pristine sample (beginning of loading, 0 contact pressure) features three peaks. The peaks

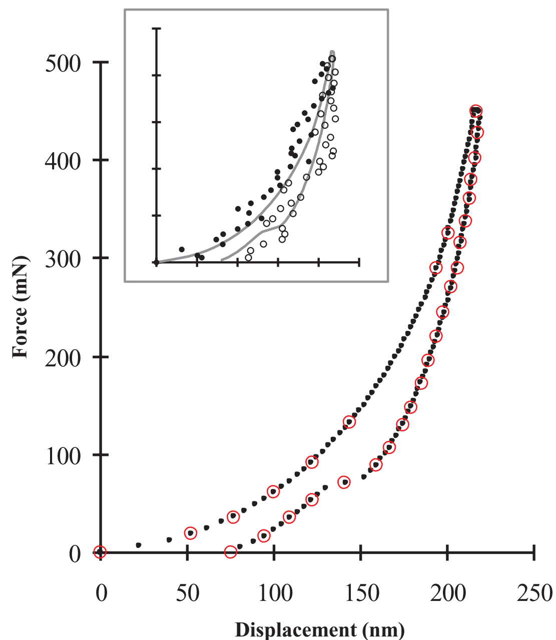

FIG. 4. (Color online) Force-displacement curve recorded with commercial indentation device on the SOS sample. The open circles marked the force values at which the Raman spectra were measured in the *in situ* experiment. The inset shows the force-displacement data recorded with the *in situ* indenter: Data collected during the loading and unloading segments are shown as solid and open symbols, respectively. The scatter in the data reflects the noise in the displacement channel. The superimposed line shows the indentation curve recorded with the commercial device. The units of the axes in the inset are the same as in the main graph.

located at 378 and 418 cm^{-1} can be assigned to the E_g and A_{1g} modes of the sapphire substrate, respectively.[43] Unstressed Si in the dc phase possesses a single, triply degenerate, Raman-active optical phonon. Nonhydrostatic stress, such as generated by an indentation contact, lowers the symmetry of the crystal and the degeneracy splits onto a singlet mode and doublet mode which causes shifts of the phonon frequency. These shifts cannot usually be resolved experimentally and the original, degenerate, Raman peak appears as a single, shifted and broadened, peak under nonhydrostatic stress, reflecting the sum of the split nondegenerate peaks. The single peak at 522.3 cm^{-1} associated with this combined mode is shifted by about 2 cm^{-1} upward from the value usually measured on bulk Si samples with Raman spectroscopy,[15,21] which indicates the presence of compressive stress in the film.[47] It is well known that Si films are compressed in plane when grown epitaxially on sapphire due to the mismatch in the crystal lattice and the difference in the thermal expansion coefficient between Si and sapphire.[48,49] Assuming a biaxial stress state,[47] the value of compressive stress in the investigated sample was calculated to be 0.8 GPa, which is similar to values reported in Raman studies on SOS films by other groups.[48–50]

On loading, significant changes in the Raman spectrum of the SOS sample were observed: At a contact pressure of 3.1 GPa, a peak (marked with A) appeared in the spectrum at 535 cm^{-1} and formed a shoulder on the right-hand side of the dc peak. As this peak is neither characteristic of Si-I nor of sapphire, it was a sign of the formation of an additional Si phase in the contact region (i.e., primary phase transformation). This phase transformation occurred at a significantly smaller contact pressure than observed under hydrostatic conditions.[5] A second peak (marked with B) located at 366 cm^{-1} appeared in the spectrum at a contact pressure of 6.1 GPa. This peak is also not associated with the Raman spectrum of Si-I or sapphire. The positions of both peaks A and B shifted continuously to higher frequencies with increasing pressure. As the height of the two peaks A and B increased with rising contact pressure, the height (signal) of the Si-I peak decreased, indicating a gradual transformation of the Si structure in the contact region. Interestingly, no plateaulike discontinuity, or so-called "pop-in" event, was found in the loading segment, in contrast to previous studies on Si with spherical indenters.[14,17,23,51] Bradby *et al.*[28] suggested that the pop-in event is a manifestation of a sudden extrusion of highly plastic transformed material from underneath the indenter. As the contact region in this work was significantly larger, due to the larger curvature radius of the indenter compared to the indenters in the above-mentioned studies, the material extrusion from underneath the indenter might not be feasible under the employed experimental conditions.

On unloading, the positions of the frequencies of modes A and B shifted to lower values, almost perfectly retracing the frequency-pressure plot of the loading segment, as shown by comparing Figs. 6 and 7. When the pressure was decreased to around 6 GPa, the Raman spectrum altered significantly, marking the start of the secondary phase transformation. The secondary phase transformation initiated at a smaller transition pressure than observed in DAC tests.[7,8] A large peak marked with C appeared at around 365 cm^{-1}. This alteration in the spectrum was not caused by a sudden increase in the signal for the phonon related to peak B; a discontinuity in the corresponding frequency-pressure plot, as shown in Fig. 7, at 6 GPa indicates that peak C represents the Raman mode of a uniquely formed phase. At the same contact pressure, a more subtle discontinuity in the derivative of the frequency-pressure plot of peak A gives further evidence for the ongoing transformation processes, which it is not as easily noticed in the Raman spectrum as in the case of peak B (see Figs. 5 and 7). More observable proof of the initiation of a different phase was the occurrence of two peaks D and E at 407 and 464 cm^{-1}, respectively. On further release of pressure, a peak F appeared in the spectrum at 391 cm^{-1}. The intensities of peaks C, D, E, and F increased with decreasing contact pressure, indicating larger portions of the material in the deformation zone converting to the formed structures. The frequencies of the modes associated with the formed phases shifted to lower values with decreasing pressure. After complete unloading, the recorded Raman spectrum was very similar to spectra recorded on residual indentation imprints in bulk Si samples, as shown in other studies.[14,52,53]

The force at which the abrupt change was observed in the spectrum on unloading was in proximity to the discontinuity (so called "pop-out") in the force-displacement curve (see Fig. 4). This provides experimental evidence for previous assumptions that this pop-out event is related to the sudden growth of substantial volumes of high-pressure phases in secondary phase transformations.[14,19,21,54]

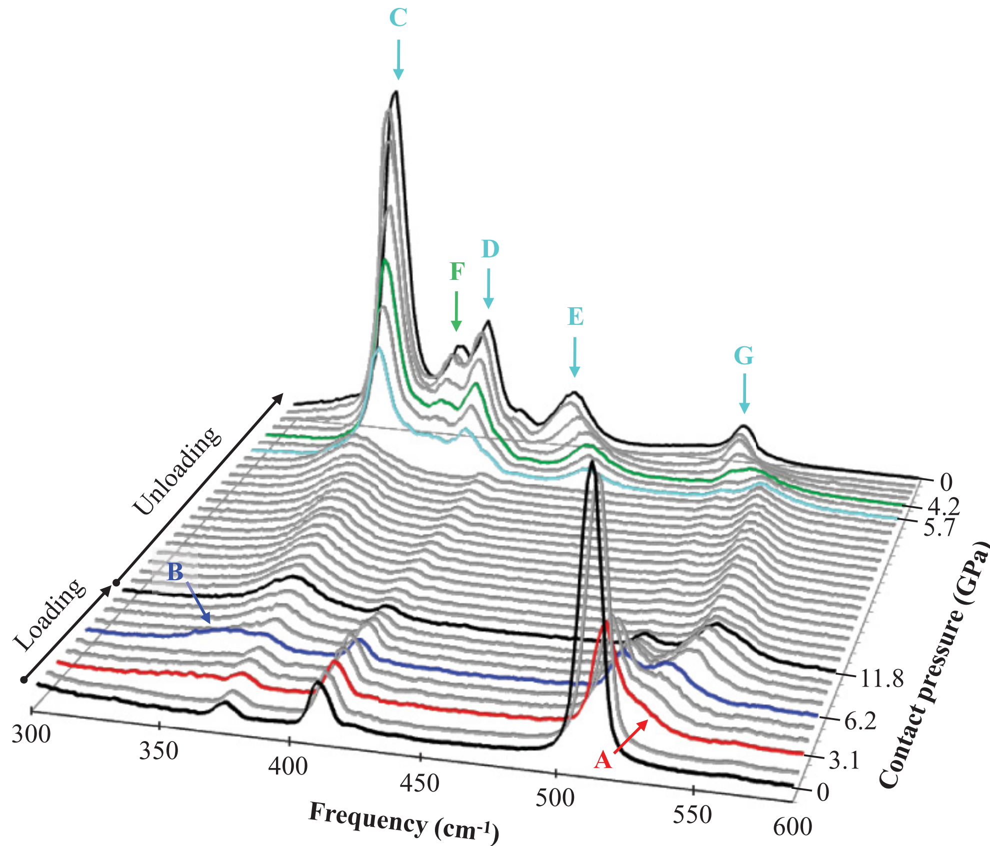

FIG. 5. (Color online) Raman spectra collected during indentation of a SOS sample at different contact pressures. Peak A has been assigned to the bct5 phase. Peak B can be assigned to bct5 as well as the β-tin phase. Peak G is associated with r8 phase, and peaks D and F with bc8 phase. Peaks E and C can represent modes from either bc8 or r8.

IV. DISCUSSION

The primary phase transformation of Si is usually characterized by a complete disappearance of the Raman mode of the Si-I phase.[18,53] In this paper, a weak signal of this mode is detected through the *in situ* experiments (see Fig. 5). This mode cannot be attributed to the dc structure preserved in the transformation zone, as was observed in a previous study.[22] The region of preserved dc structure would be exposed to very large compressive stresses during loading, and hence the mode of Si-I would be expected to shift to significantly higher frequencies.[22,53,55] However, the frequency of the mode changed only marginally with increasing pressure in this study [see Fig. 6(a)]. Therefore, it is mostly likely that the residual dc peak originated from the untransformed material surrounding the deformed contact region (see Fig. 3).

The shifts of those Raman modes related to the primary transformation are summarized and compared to data available in literature for the investigated frequency and pressure range in Fig. 6(b). The cited experimental study describes the phase transformation of Si powder (dc phase) into β-tin during hydrostatic compression tests in DAC.[56] The theoretical studies focus on calculations of the pressure-induced Raman shifts for β-tin during DAC tests.[57–59] The frequency-pressure plot of peak B aligns reasonably well with data for the doubly degenerate transverse optical (TO) mode of β-tin reported in these papers [shown in Fig. 6(b)]. This mode corresponds to the opposing motion of the two interpenetrating bct sublattices in directions perpendicular to the β-tin [001] axis.[58] Indentation of the sample caused the sublattices to slide against each other, resulting in the shift in the frequencies of this mode. Beside β-tin, no further phases, hence, no modes in the frequency range of peak A, were found in the explored pressure range in hydrostatic studies. However, in indentation simulations (under the presence of shear strain), the formation of another phase, bct 5, was observed by various groups,[32–35] as mentioned previously. Two Raman-active modes with E_g and A_{1g} symmetries were predicted for the bct5 phase with frequencies of 520 and 340 cm^{-1}.[11,60] The calculated E_g frequency for the bct5 phase is in the frequency range of peak A, suggesting the formation of this phase in the deformed region. This would be experimental evidence for this phase. The frequencies for the A_{1g} mode of bct5 and the TO mode of β-tin are similar which makes an unambiguous assignment of peak B to either of these phases extremely difficult. It was assumed that both phases were present in the deformation zone, as recent simulations predict the concurrent transformation of the Si-I phase to β-tin and bct5 structures during indentation loading,[25,32–35] The dc

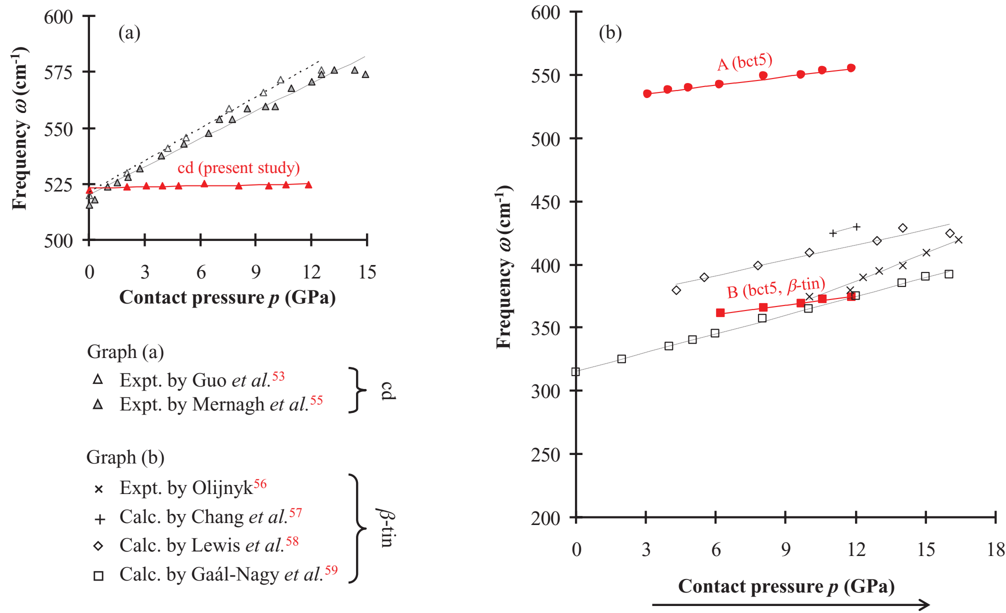

FIG. 6. (Color online) Pressure dependence of the frequencies for (a) Raman mode of dc Si-I and (b) Raman modes assigned to transformed Si structures during the loading segment of indentation. Peak A has been assigned to the bct5 phase. Peak B can be assigned to bct5 as well as the β-tin phase. For comparison purposes, data from other experimental (Expt.) and theoretical (Calc.) studies are included. The lines are guides for the eye.

structure transforms to the β-tin structure by compressing the dc face-centered-cubic sublattices and shifting them relatively to each other in opposite directions along the slip planes.[32,61] In this tetragonal transformation, the angles of the unit cell remain unchanged, while the lengths of the unit-cell axes are contracted along the coincident dc [001] and β-tin [001] axes and extended along the coincident dc $\langle 110 \rangle$ and β-tin [100] axes, without breaking the bonds between atoms.[32] The transformation leads to nearly ideal sixfold Si coordination with the two formed bonds in the [001] directions slightly longer than those from the original fourfold coordination.[36] In case of the bct5 formation, the length of the unit-cell axes remains almost invariant and the lattice angles are modified;[32] the transformation is dominated by contraction along the dc [3,14,3] direction and expansion along the $[1,0,\bar{1}]$ direction.[32] The initially stepped sixfold rings of the dc (110) lattice planes are flattened and produce the densely packed (110) plane of the bct5 lattice without any bond breaking.[32] The bct5 structure is created by three flattened adjacent planes with two planes being shifted against each other to create the fifth bond in the unit cell, leading to nearly ideal fivefold Si coordination; the bonds in the bct5 [001] direction are slightly shorter than the other four bonds.[32] To determine unequivocally the formation of β-tin in the contact region, the occurrence of the longitudinal optical mode for β-tin has to be verified, which is located at around 120 cm^{-1}.[56,59] This frequency is presently outside the detection range of the Raman microscope used in this paper.

During unloading, secondary phase transformations were observed when the contact pressure decreased below a threshold value. The formed phases were identified to be bc8 and r8 based on calculations for phonon modes published by Piltz *et al.*[8] The transformation from the β-tin phase to the r8 structure requires breaking bonds along the β-tin [111] direction and bonding across to the nearest unbonded neighbors, which lie in the same direction.[7] The r8 structure is a rhombohedral distortion of the bc8 phase, where only one bonding pair has to be rearranged in the unit cell during phase transformation.[7,8] To the best of our knowledge, a transformation path from the bct5 structure to the r8 or bc8 phases has not yet been described in the literature.

As the unloading rate and unloading strain rate were relatively slow, the formation of the r8 and bc8 phases rather than a-Si was expected based on the findings of previous studies.[16,21,23] The calculated frequencies of the Raman-active modes for the r8 phase are 514 cm^{-1} (E_g), 440 cm^{-1} (E_g), 440 cm^{-1} (A_g), 350 cm^{-1} (A_g), and 337 cm^{-1} (E_g) and for the bc8 phase are 447 cm^{-1} (E_g), 404 cm^{-1} (T_u), 387 cm^{-1} (T_g), 354 cm^{-1} (A_g), and 354 cm^{-1} (T_g).[8] Accordingly, peak G was assigned to the upper phonon mode of the r8 Si-XII structure. The peaks D and F indicate the presence of bc8. Peaks E and C could be associated with either phase, as bc8 and r8 exhibit phonons with similar frequencies in this region of the Raman spectrum. The calculated phonon frequencies were found to be in good agreement with the experimental results obtained after complete unloading ($p_i = 0$ GPa). However, the r8 mode located at 337 cm^{-1} was not observed in this work; it was also not detected in studies conducted by other groups.[62–65]

The data indicate that bc8 forms (almost) simultaneously with the r8 structure in indentation tests and not subsequently to r8 formation, as previously assumed based on DAC tests, at significantly smaller contact pressures.[21] The lattices of the formed structures are severely strained, and as the strain is (at least partially) released by reducing the contact pressure, the frequency of the phonon modes shifts to lower values. The slope of the pressure-frequency plots of the observed modes are similar to those in DAC studies conducted by Hanfland *et al.*[64] and Olijnyk *et al.*[56] as shown in Fig. 7.

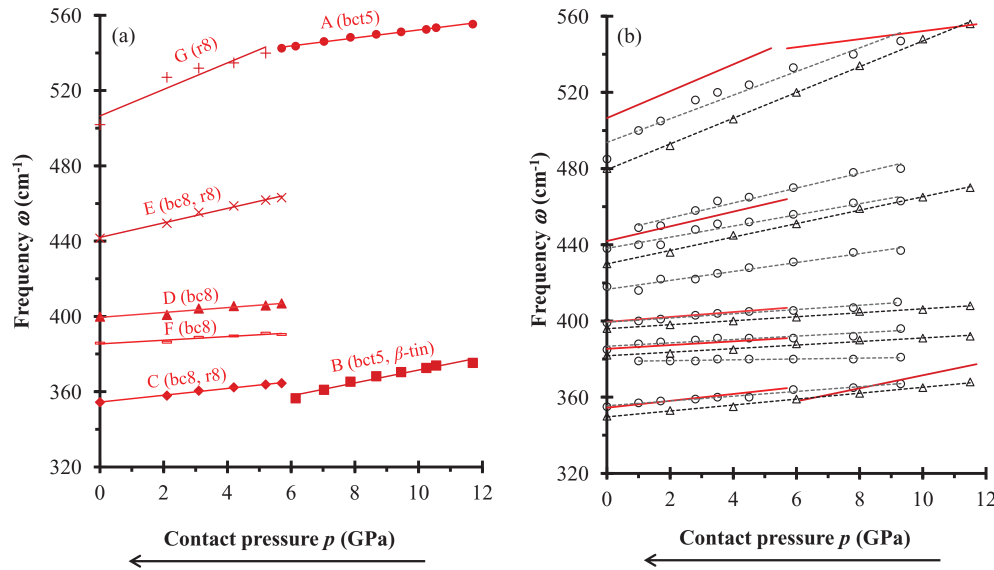

FIG. 7. (Color online) Pressure dependence of the frequencies for transformed Si structures during the unloading segment of the indentation in the present study (a). Peak A has been assigned to the bct5 phase. Peak B can be assigned to bct5 as well as the β-tin phase. Peak G is associated with r8 phase, and peaks D and F with bc8 phase. Peaks E and C can represent modes from either bc8 or r8. For comparison purposes, data from experimental studies by Olijnyk and Jephcoat (Ref. 63) (O) and by Hanfland and Syassen (Ref. 64) (△) are shown in (b). The trend lines from (a) for the Raman frequencies observed in this paper are included as solid lines in this graph. All lines are for guidance of the eye.

The primary phase transformation was initiated at a much lower peak indentation strain for the SOS sample than thought possible based on a previous study,[22] in which phase transformation was observed only at strains of at least $\varepsilon_I = 0.04$ in indentation tests. This previous study examined data compiled on bulk, single-crystal Si samples, whereas an epitaxial Si film was investigated here. The Si film exhibits a considerable amount of compressive stress (see Sec. II). It has been suggested that compressive stress would promote phase transformation in thin semiconductor films,[66] which could explain why smaller strains were required for initiating phase transformation processes.

V. CONCLUSIONS

The indentation-induced phase transformation of a Si thin film was observed *in situ* using Raman microscopy. The reported *in situ* experiments provide insights on the transformation processes in Si during indentation, both confirming and disproving some of the previous assumptions made on this subject. Experimental evidence was found for the existence of the theoretically predicted bct5 phase of Si and data on the pressure dependence of the Raman phonons for this phase were provided. Contrary to existing belief, it was revealed that the formation of r8 and bc8 occurs simultaneously and not sequentially, as had been previously thought. The findings of the formation of r8 are of special importance as it was recently predicted that this phase has a greater carrier mobility than diamond cubic Si[31] and exhibits photovoltaic absorption over a larger range of the incident solar spectrum than other Si phases.[4] The paper showed that the presence of shear stress can reduce the transition pressure for phase transformations compared to purely hydrostatic conditions and promotes the formation of phases that are not observable in DAC tests. Due to the constrained nature of the Si film, the transitions occurred at smaller strains than those exhibited for bulk, single-crystal Si materials. The findings emphasize that predictions based on findings in hydrostatic tests have only limited validity regarding the phase transformation of material exposed to more complex stress conditions. In this context, the developed experimental setup coupling indentation with *in situ* Raman microscopy has shown its usefulness in advancing the understanding of deformation mechanisms under such conditions.

ACKNOWLEDGMENTS

The authors would like to thank Mark Vaudin, Ceramics Division at the National Institute of Standards and Technology NIST, for conducting the EBSD measurements.

[1] G. M. Pharr, W. C. Oliver, and D. S. Harding, J. Mater. Res. **6**, 1129 (1991).

[2] D. R. Clarke, M. C. Kroll, P. D. Kirchner, R. F. Cook, and B. J. Hockey, Phys. Rev. Lett. **60**, 2156 (1988).

[3] R. Rao, J. E. Bradby, and J. S. Williams, Appl. Phys. Lett. **91**, 123113 (2007).

[4] B. D. Malone, J. D. Sau, and M. L. Cohen, Phys. Rev. B **87**, 161202(R) (2008).

[5] R. J. Needs and A. Mujica, Phys. Rev. B **51**, 9652 (1995).
[6] A. Mujica, A. Rubio, A. Munoz, and R. J. Needs, Rev. Mod. Phys. **75**, 863 (2003).
[7] J. Crain, G. J. Ackland, J. R. Maclean, R. O. Piltz, P. D. Hatton, and G. S. Pawley, Phys. Rev. B **50**, 13043 (1994).
[8] R. O. Piltz, J. R. Maclean, S. J. Clark, G. J. Ackland, P. D. Hatton, and J. Crain, Phys. Rev. B **52**, 4072 (1995).
[9] J. Gilman, Philos. Mag. B **67**, 207 (1993).
[10] W. C. D. Cheong and J. C. Zhang, Key Eng. Mater. **233–236**, 603 (2003).
[11] L. L. Boyer, E. Kaxiras, J. L. Feldman, J. Q. Broughton, and M. J. Mehl, Phys. Rev. Lett. **67**, 715 (1991).
[12] K. Mylvaganam, L. C. Zhang, P. Eyben, J. Mody, and W. Vandervorst, Nanotechnology **20**, 305705 (2009).
[13] S.-T. Ho, Y.-H. Chang, and H.-N. Lin, J. Appl. Phys. **96**, 3562 (2004).
[14] J. E. Bradby, J. S. Williams, J. Wong-Leung, M. V. Swain, and P. Munroe, J. Mater. Res. **16/5**, 1500 (2001).
[15] A. Kailer, Y. G. Gogotsi, and K. G. Nickel, J. Appl. Phys. **81**, 3057 (1997).
[16] J. Jang, M. J. Lance, S. Wen, T. Y. Tsui, and B. M. Pharr, Acta Mater. **53**, 1759 (2005).
[17] H. Saka, A. Shimatani, M. Suganuma, and Suprijadi, Philos. Mag. A **82**, 1971 (2002).
[18] D. Ge, Ph.D. thesis, Drexel University, 2004.
[19] I. Zarudi, L. C. Zhang, J. Zou, and T. Vodenitcharova, J. Mater. Res. **19**, 332 (2004).
[20] A. Haq and P. R. Munroe, J. Mater. Res. **24**, 1967 (2009).
[21] V. Domnich and Y. Gogotsi, Rev. Adv. Mater. Sci. **3**, 1 (2002).
[22] Y. B. Gerbig, S. J. Stranick, and R. F. Cook, Phys. Rev. B **83**, 205209 (2011).
[23] Y. B. Gerbig, S. J. Stranick, D. J. Morris, M. D. Vaudin, and R. F. Cook, J. Mater. Res. **24**, 1172 (2009).
[24] I. Zarudi, L. C. Zhang, W. C. D. Cheong, and T. X. Yu, Acta Mater. **53**, 4795 (2005).
[25] P. Eyben, F. Clemente, K. Vanstreels, G. Purtois, T. Clarysse, K. Sankaran, J. Mody, W. Vandervorst, K. Mylvaganam, and L. Zhang, J. Vac. Sci. Technol. B **28**, 401 (2010).
[26] I. V. Gridneva, Y. V. Milman, and V. I. Trefilov, Phys. Status Solidi **14**, 77 (1972).
[27] M. C. Gupta and A. L. Ruoff, J. Appl. Phys. **51**, 1072 (1980).
[28] J. E. Bradby, J. S. Williams, and M. V. Swain, Phys. Rev. B **67**, 085205 (2003).
[29] S. Ruffell, J. E. Bradby, J. S. Williams, R. C. Major, and O. L. Warren, Mater. Res. Soc. Symp. Proc. **1146**, 1146-NNO2-06 (2009).
[30] A. B. Mann, D. Van Heerden, J. B. Pethica, P. Bowes, and T. P. Weihs, Philos. Mag. A **82**, 1921 (2002).
[31] B. D. Malone, J. D. Sau, and M. L. Cohen, Phys. Rev. B **78**, 035210 (2008).
[32] D. E. Kim and S. I. Oh, J. Appl. Phys. **104**, 013502 (2008).
[33] Y.-H. Lin, S.-R. Jian, Y.-S. Lai, and P.-F. Yang, Nanoscale Res. Lett. **2**, 71 (2008).
[34] C. F. Sanz-Navarro, S. D. Kenny, and R. Smith, Nanotechnology **15**, 692 (2004).
[35] G. S. Smith, E. B. Tadmor, N. Bernstein, and E. Kaxiras, Acta Mater. **49**, 4089 (2001).
[36] E. Kaxiras and L. L. Boyer, Modell. Simul. Mater. Sci. Eng. **1**, 91 (1992).
[37] S. Ruffell, J. E. Bradby, J. S. Williams, and O. L. Warren, J. Mater. Res. **22**, 578 (2007).
[38] Any mention of commercial products within this paper is for information only; it does not imply recommendation or endorsement by NIST.
[39] T. C. Damen, S. P. S. Porto, and B. Tell, Phys. Rev. **142**, 570 (1966).
[40] J. J. Parise, L. L. Howell, and S. P. Magleby, Mech. Mach. Theory **36**, 1281 (2001).
[41] C. A. Michaels, J. Raman Spectrosc. **41**, 1670 (2010).
[42] T. Wermelinger, C. Borgia, C. Solenthaler, and R. Spolenak, Acta Mater. **55**, 4657 (2007).
[43] G. H. Watson Jr., W. B. Daniels, and C. S. Wang, J. Appl. Phys. **52**, 956 (1981).
[44] E. R. Weppelmann, J. S. Field, and M. V. Swain, J. Mater. Res. **8**, 830 (1993).
[45] J. S. Field and M. V. Swain, J. Mater. Res. **8**, 297 (1993).
[46] D. Tabor, *The Hardness of Metals* (Clarendon, Oxford, UK, 1951).
[47] I. De Wolf, Semicond. Sci. Technol. **11**, 139 (1996).
[48] H. S. Mavi, A. K. Shukla, K. P. Jain, S. C. Abbi, and R. Beserman, J. Appl. Phys. **69**, 7815 (1991).
[49] G. A. Sai-Halasz, F. F. Fang, T. O. Sedgwick, and A. Segmüller, Appl. Phys. Lett. **36**, 419 (1980).
[50] K.-I. Yamazaki, M. Yamada, K. Yamamoto, and K. Abe, Jpn. J. Appl. Phys. **23**, 681 (1984).
[51] T. Juliano, V. Domnich, and Y. Gogotsi, J. Mater. Res. **19**, 3099 (2004).
[52] D. Ge, V. Domnich, and Y. Gogotsi, J. Appl. Phys. **93** 2418 (2003).
[53] J. J. Guo, D. Pan, X. Q. Yan, T. Fujita, and M. W. Chen, Appl. Phys. Lett. **96**, 251910 (2010).
[54] S. Ruffell, J. E. Bradby, J. S. Williams, and P. Munroe, J. Appl. Phys. **102**, 063521 (2007).
[55] T. P. Mernagh and L.-G. Liu, J. Phys. Chem. Solids **52**, 507 (1991).
[56] H. Olijnyk, Phys. Rev. Lett. **68**, 2232 (1992).
[57] K. J. Chang, and M. L. Cohen, Phys. Rev. B **31**, 7819 (1985).
[58] S. P. Lewis and M. L. Cohen, Phys. Rev. B **48**, 3646 (1993).
[59] K. Gaál-Nagy, M. Schmitt, P. Pavone, and D. Strauch, Comput. Mater. Sci. **22**, 49 (2001).
[60] E. Kaxiras and L. L. Boyer, Phys. Rev. B **50**, 1535 (1994).
[61] S. M.-M. Dubois, G.-M. Rignanese, T. Pardoen, and J.-C. Charlier, Phys. Rev. B **74**, 235203 (2006).
[62] Y. B. Gerbig, S. J. Stranick, and R. F. Cook, Scr. Mater. **63**, 512 (2010).
[63] H. Olijnyk and A. P. Jephcoat, Phys. Status Solidi B **211**, 413 (1999).
[64] M. Hanfland and K. Syassen, High Press. Res. **3**, 242 (1990).
[65] G. Weill, J. L. Mansot, G. Sagon, C. Carlone, and J. M. Besson, Semicond. Sci. Technol. **4**, 280 (1989).
[66] D. J. Oliver, J. E. Bradby, J. S. Williams, M. V. Swain, and P. Munroe, Nanotechnology **19**, 475709 (2008).